

BROADBAND PHYSICS-BASED MODELING OF MICROWAVE PASSIVE DEVICES THROUGH FREQUENCY MAPPING

John W. Bandler,^{1,2} Mostafa A. Ismail¹ and José E. Rayas-Sánchez¹

¹Simulation Optimization Systems Research Laboratory, Department of Electrical and Computer Engineering, McMaster University, Hamilton, Ontario, Canada L8S 4K1; e-mail: bandler@mcmaster.ca

²Bandler Corporation, P.O. Box 8083, Dundas, Ontario, Canada L9H 5E7; e-mail: john@bandler.com

ABSTRACT: We present a new computer-aided modeling methodology to develop physics-based models for passive components. We coherently integrate full-wave EM simulators, artificial neural networks, multivariable rational functions, dimensional analysis and frequency mapping to establish broadband models. We consider both frequency-independent and frequency-dependent empirical models. Frequency mapping is used to develop the frequency-dependent empirical models. Useful properties of the frequency mapping are also presented and utilized in the modeling process. We also consider the transformation from frequency-dependent models into frequency-independent ones. The passivity of the frequency-dependent empirical model is also considered. We illustrate the modeling process through various examples, including a microstrip right angle bend, a microstrip via, a microstrip double-step (to be used as a basic element of constructing a model for nonuniform or tapered microstrip transmission lines) and a CPW step junction.

Keywords: empirical models, modeling, passive devices, frequency mapping, rational functions, neural Networks

I. INTRODUCTION

We present a new computer-aided modeling methodology to develop physics-based empirical models for microwave passive components. We integrate in a coherent way EM simulators, artificial neural networks [1,2], multivariable rational functions [3], dimensional analysis [4,5] and frequency mapping [6,7] to establish models valid over broad frequency ranges. We consider frequency-independent empirical models (FIEM) and frequency-dependent empirical models (FDEM). In the FDEM we use the frequency mapping approach [6,7] which implicitly introduces frequency dependency into the model elements. We also exploit the odd property of the frequency mapping, that is the

transformed frequency must be an odd function of the original frequency. Artificial neural networks or rational functions are used to approximate these elements as well as the frequency mapping. Rational functions enable us to transform a simple FDEM to an equivalent FIEM. This transformation can be expedited by impedance synthesis [8] as we will see in the examples. The passivity of the FDEMs is also considered. Dimensional analysis [4,5] determines the functionality of the model elements and the frequency mapping on the components' geometrical and physical parameters. It also reduces the amount of training data required in the approximation process. The data required to develop the empirical models is obtained by accurate but time intensive full-wave EM simulators (referred to in the space mapping literature as “fine” models [6]). We illustrate the process through various examples, including a microstrip right angle bend, a microstrip via, a microstrip double-step (to be used as a basic element of constructing a model for nonuniform or tapered microstrip transmission lines) and a CPW step junction.

Equivalent circuits can be obtained from the literature or can be visualized by microwave engineers through their understanding and expertise of microwave components. We believe that, though simple, they have advantages over black-box modeling of microwave components since they embody physical characteristics (at least at low frequencies) of the actual components. A shortcoming is that those equivalent circuits may fail to give good accuracy at high frequencies due to dispersion. We address dispersive effects by introducing the frequency dependency into the elements of the equivalent circuits.

II. FREQUENCY INDEPENDENT EMPIRICAL MODELS (FIEM)

Consider a microwave component modeled by a fine model (typically a full-wave EM simulator) and a circuit model (empirical model). We assume that the topology of the equivalent circuit is known but the empirical formulas of their elements are to be determined. This concept is shown in Fig. 1. The vector \mathbf{x}_f is an n -dimensional vector representing the parameters of the microwave component and ω is the frequency. The vectors \mathbf{R}_f and \mathbf{R}_c represent the fine and circuit model responses, respectively. The development of the FIEM is shown in Fig. 2. The vector \mathbf{y} is an l -dimensional vector representing the

empirical formulas of the elements of the circuit model. Applying dimensional analysis [4,5] the vector \mathbf{y} becomes a function of an n_r -dimensional vector \mathbf{x}_r ($n_r < n$), which we call the reduced input parameter vector (we will show in the examples how to construct this vector). We approximate \mathbf{y} through artificial neural network [1, 2] or multivariable rational functions [3] in a certain region of parameters and frequency as

$$\mathbf{y} \approx \mathbf{Q}(\mathbf{x}_r, \mathbf{w}) \quad (1)$$

where \mathbf{w} is a set of unknown parameters. The set \mathbf{w} is evaluated by solving the optimization problem

$$\min_{\mathbf{w}} \left\| [\mathbf{e}_{11}^T \cdots \mathbf{e}_{1M}^T \mathbf{e}_{21}^T \cdots \mathbf{e}_{2M}^T \cdots \mathbf{e}_{N1}^T \cdots \mathbf{e}_{NM}^T]^T \right\| \quad (2)$$

where $\| \cdot \|$ is a suitable norm, N is the total number of training points, M is the number of frequency points per frequency sweep and \mathbf{e}_{ij} is an error vector given by

$$\mathbf{e}_{ij} = \mathbf{R}_f(\mathbf{x}_{f_i}, \omega_j) - \mathbf{R}_c(\mathbf{Q}(\mathbf{x}_{r_i}, \mathbf{w}), \omega_j) \quad (3)$$

The optimization problem in (2) is solved by the Huber optimizer implemented in OSA90 [13]. The training points are selected according to the Central Composite Design [9] and more training points are added if necessary.

III. FREQUENCY DEPENDENT EMPIRICAL MODELS (FDEM)

Two approaches can be used to introduce frequency dependency to the elements of the FDEM. One approach is to introduce the frequency dependency directly to the vector \mathbf{y} (Fig. 3). The second approach exploits the frequency mapping (transformation) concept [6,7], where we simulate the circuit model at a different frequency from the fine model. We call this frequency the circuit model frequency ω_c . Frequency mappings (transformations) have roots in classical filter design, for example, low-pass to band-pass or high-pass transformations [10]. The development of the FDEM using this approach is shown in Fig. 4. The dependency of ω_c on ω as well as the physical parameters is determined by applying dimensional analysis. Artificial neural networks or multivariable rational functions are used to approximate \mathbf{y} and ω_c

$$\mathbf{y} \approx \mathbf{Q}(\mathbf{x}_r, \mathbf{w}_1) \quad (4a)$$

$$\omega_c \approx \Omega(\mathbf{x}_r, \omega, \mathbf{w}_2) \quad (4b)$$

where \mathbf{w}_1 and \mathbf{w}_2 are unknown parameters. These parameters are evaluated by solving the optimization problem in (2) with the error vector \mathbf{e}_{ij} given by

$$\mathbf{e}_{ij} = \mathbf{R}_f(\mathbf{x}_{f_i}, \omega_j) - \mathbf{R}_c(\mathbf{Q}(\mathbf{x}_{r_i}, \mathbf{w}_1), \Omega(\mathbf{x}_{r_i}, \omega_j, \mathbf{w}_2)) \quad (5)$$

Properties of the Frequency Mapping

Simulating the circuit model at a different frequency from that of the fine model is an implicit way of introducing frequency dependency to the elements of the circuit model. For example, if the device is lossless the circuit model contains only lossless lumped-elements (inductors and capacitors). In this case, a FDEM simulated at ω_c and with a circuit element vector \mathbf{y} is equivalent to a FDEM simulated at ω and with a circuit elements vector \mathbf{y}_1 given by

$$\mathbf{y}_1 = (\omega_c / \omega) \mathbf{y} \quad (6)$$

This can be proved as follows. For any inductor L and capacitor C (simulated at frequency ω_c) in \mathbf{y} we have

$$Z_L = j \omega (L \omega_c / \omega) \quad (7a)$$

$$Y_c = j \omega (C \omega_c / \omega) \quad (7b)$$

Therefore, the circuit elements vector \mathbf{y}_1 (simulated at frequency ω) is related to the vector \mathbf{y} by (6). Furthermore, the frequency ω_c should be an odd function of ω . This results from the even and odd properties [10] of an arbitrary frequency-dependent impedance $Z(\omega)$, where the real (imaginary) part should be an even (odd) function of frequency. For example, if an inductor L is simulated at frequency ω_c the equivalent impedance $Z_L = j \omega_c L$ is purely imaginary, hence Z_L and consequently ω_c should be odd function of ω . The odd property is also preserved when using the frequency mapping to transform a low-pass filter into a high- or a band-pass filter [10]. We use this property in conjunction with dimensional analysis to further reduce the number of parameters of the artificial neural network or the multivariable rational function approximating ω_c .

Transformation of FDEMs into FIEMs

The advantage of using a multivariable rational function to approximate the frequency mapping is that we can transform the FDEM into an equivalent FIEM. This transformation involves one-port impedance synthesis, which states that the impedance we want to realize should be a positive real rational function [8]. For example, the impedances associated with an inductor L and a capacitor C (simulated at ω_c) in the circuit elements vector \mathbf{y} are $Z_L = j\omega_c L$ and $Z_C = 1/j\omega_c C$, respectively. Those impedances can be realized using any of the one-port impedance synthesis techniques such as the first Foster realization or second Foster realization or ladder realization [8]. In the examples presented here, we notice that the frequency ω_c takes the form

$$\omega_c = \omega \frac{f_1 - \omega^2 f_2}{f_3 - \omega^2 f_4} \quad (8)$$

where f_1, f_2, f_3, f_4 are functions of the device physical parameters. Therefore, the impedances associated with an inductor L and a capacitor C in the circuit elements vector \mathbf{y} are given by

$$Z_L = j \omega L \frac{f_1 - \omega^2 f_2}{f_3 - \omega^2 f_4} \quad (9a)$$

$$Z_C = \frac{1}{j\omega} \frac{f_3 - \omega^2 f_4}{f_1 - \omega^2 f_2} \quad (9b)$$

We believe that (8) may be useful for other devices such as microstrip mitered bends, microstrip step junctions, etc.

Passivity of the FDEMs

The FDEM of a microwave component is passive if the equivalent impedance of each element (inductor or capacitor) of the circuit model is realizable. That is, the equivalent impedances given by (9a) and (9b) are realizable. An impedance $Z(s)$, where $s = j\omega$, is realizable if and only if it is a positive real function of s , i.e, $Z(s)$ is a real rational function of s and $\text{Re}(Z(s)) \geq 0$ if $\text{Re}(s) \geq 0$ [8]. For an LC impedance this implies that all poles of $Z(s)$ are simple and lie on the $j\omega$ axis and have positive real residues. Applying these conditions on the impedance in (9a) and (9b) and performing some algebraic manipulations we get the passivity conditions of the FDEMs (see Appendix A). A FDEM is passive if the

circuit elements (inductors and capacitors) are positive and the parameters of the frequency mapping in (8) satisfy

$$f_i > 0, \quad i = 1 \dots 4 \quad (10a)$$

$$\begin{vmatrix} f_1 & f_2 \\ f_3 & f_4 \end{vmatrix} > 0 \quad (10b)$$

Therefore in order to insure the passivity of the FDEMs (10a) and (10b) should be included as constraints to the optimization problem in (2).

IV. MULTIVARIABLE RATIONAL FUNCTIONS

Multivariable rational functions (MRFs) [3] are used in most of the modeling examples developed here. A multivariable rational function is the quotient of two polynomials,

$$f(\mathbf{x}, \mathbf{a}, \mathbf{b}) = \frac{a_0 + \sum_{i=1}^n a_i x_i + \sum_{i=1}^n \sum_{j \geq i}^n a_{ij} x_i x_j + \dots}{1 + \sum_{i=1}^n b_i x_i + \sum_{i=1}^n \sum_{j \geq i}^n b_{ij} x_i x_j + \dots} \quad (11)$$

where $\mathbf{x} = [x_1 \ x_2 \ \dots \ x_n]^T$ is the input vector and \mathbf{a} , \mathbf{b} are two vectors containing the unknown a 's and b 's respectively. The polynomials in the numerator and the denominator are of finite order p and q , respectively. The rational function in (11) is fully characterized by the number of input variables n , the numerator order p and the denominator order q , hence we refer to it as $\text{MRF}_{n,p,q}$. The number of unknown parameters in \mathbf{a} and \mathbf{b} can be reduced if some of the input variables are restricted to a certain order less than p or q . For example, a $\text{MRF}_{2,3,2}$ with the order of the input variable x_1 restricted to 1 is given by

$$f(\mathbf{x}, \mathbf{a}, \mathbf{b}) = \frac{a_0 + a_1 x_1 + a_2 x_2 + a_{12} x_1 x_2 + a_{22} x_2^2 + a_{122} x_1 x_2^2 + a_{222} x_2^3}{1 + b_1 x_1 + b_2 x_2 + b_{12} x_1 x_2 + b_{22} x_2^2} \quad (12)$$

which has 11 unknown parameters. On the other hand, the full $\text{MRF}_{2,3,2}$ has 15 unknown parameters. The unknown parameters in \mathbf{a} and \mathbf{b} can be computed by two methods. First, if the values of the function f in (11) are explicitly available we can evaluate \mathbf{a} and \mathbf{b} by solving a system of linear equations. This is done by applying cross-multiplication to both sides of (11) and rearranging the terms to get a system of linear equations in the elements of \mathbf{a} and \mathbf{b} . This system of linear equations can be solved by the method

of least-squares or recursive least-squares algorithm [3]. Second, if values of f are not directly available we evaluate \mathbf{a} and \mathbf{b} by solving a suitable optimization problem (in our case the optimization problem in (2)). The second method is adopted in this work since we evaluate the elements of the empirical model (inductors, capacitors, the frequency ω_c) and the only available information are the scattering parameters supplied by the EM simulators.

V. MODELING EXAMPLES

To display the results in a compact way we define the error in the scattering parameter S_{ij} as the modulus of the difference between the scattering parameter S_{ij}^f computed by the fine model and the scattering parameter S_{ij}^c computed by the circuit model

$$\text{error in } S_{ij} = |S_{ij}^f - S_{ij}^c| = \sqrt{(\text{Re}[S_{ij}^f] - \text{Re}[S_{ij}^c])^2 + (\text{Im}[S_{ij}^f] - \text{Im}[S_{ij}^c])^2} \quad (13)$$

where $i = 1, 2, \dots, P$ and $j = 1, 2, \dots, P$ (P is the number of ports of the microwave device). We also define the percentage error in S_{ij} by

$$\% \text{ error in } S_{ij} = \left| \frac{S_{ij}^f - S_{ij}^c}{S_{ij}^f} \right| \times 100 \quad (14)$$

We will use percentage error in S_{ij} to display the results whenever $|S_{ij}^f|$ is not zero.

Microstrip Right Angle Bend

Here, we develop a frequency-independent and frequency-dependent empirical model for the microstrip right angle bend in Fig. 5(a). The fine model is analyzed by Sonnet's *em* [11] and the circuit model is the LC circuit [12] in Fig. 5(b). The vector of input parameters $\mathbf{x}_f = [W \ H \ \varepsilon_r]^T$ and the vector of the circuit elements is $\mathbf{y} = [L/H \ C/H]^T$. Applying dimensional analysis [4,5], we can show that \mathbf{y} is related to \mathbf{x}_f by

$$L/H = \mu_0 f(W/H) \quad (15a)$$

$$C/H = \varepsilon_0 f(W/H, \varepsilon_r) \quad (15b)$$

Therefore, \mathbf{y} is a function of $\mathbf{x}_r = [W/H \ \varepsilon_r]^T$. We first develop a FIEM in the frequency range [1, 11] GHz. The region of interest is $0.2 < W/H < 6$ and $2 < \varepsilon_r < 11$. The substrate height H is chosen in the range [5, 30] mil. We use a three-layer perceptron ANN (with hyperbolic-tangent as nonlinear activation function) to approximate \mathbf{y} . Two hidden neurons were used for L/H and three hidden neurons for C/H . The training points are chosen according to the Central Composite Design [9] in addition to 4 more points as shown in Fig. 6 (total 13 training points) where \hat{x}_1 and \hat{x}_2 are the scaled input variables corresponding to W/H and ε_r , respectively. The vector \mathbf{y} is also approximated by multivariable rational functions. The inductance per unit length L/H is approximated by a rational function $\text{MRF}_{2,2,2}$ and the capacitance per unit length C/H is approximated by a rational function $\text{MRF}_{2,3,0}$ with the order of W/H restricted to one (this gives better generalization performance than if we did not restrict the order of W/H). The parameters of the ANNs and the MRFs are obtained by the Huber optimizer in OSA90/hope [13]. Figs. 7(a) and (b) show the error in the scattering parameter S_{11} at 16 test points in the region of interest for the FIEM developed by ANN and MRF, respectively. Fig. 7(c) shows the corresponding error due to the Jansen model [14] at the same test points. We see that the three models are comparable.

The results obtained by the FIEM (developed by either ANNs or MRFs) and by the Jansen empirical model [14] over broad frequency range are shown in Figs. 8 (a), (b) and (c), respectively. It is clear that neither the FIEM nor the empirical model in [14] are accurate at high frequencies. Therefore, we develop a FDEM (see Fig. 4), where ω_c is a function of ω and the other parameters. Applying dimensional analysis (see Appendix B) and using the odd property of ω_c we get

$$\omega_c = \omega \gamma(\mathbf{x}_r, (\omega H/c)^2) \quad (16)$$

where c is the speed of light and γ is an unknown function to be approximated. We use multivariable rational functions to approximate \mathbf{y} as well as ω_c . A $\text{MRF}_{3,2,2}$ with the order of $(\omega H/c)^2$ restricted to one is used to approximate ω_c . The number of training points used to develop the FDEM is the same as that used to develop the FIEM. Figs. 9 (a) and (b) show the errors in the scattering parameters S_{11} and S_{21} at

16 test points in the region of interest for the FDEM. Fig. 10 compares the results obtained by the FDEM and those from Sonnet's *em* [11]. The empirical expressions for y and ω_c are given in Table I.

We transform the FDEM into an equivalent FIEM as follows. The frequency ω_c is given by (8) and, hence the impedances associated with L and C are given by (9a) and (9b), respectively. These impedances are realized by the first Foster realization [8]. The equivalent FIEM is shown in Fig. 11(b), where all elements are frequency independent and functions only of the device parameters.

Microstrip Via

Here, we consider modeling the microstrip via of Fig. 12(a). The circuit model is an inductor L to ground (Fig. 12(b)). The fine model is analyzed by Sonnet's *em* [11]. The reference plane is at the junction of the microstrip line and the square pad. The vector $\mathbf{x}_f = [W/H \ W_0/W \ D/W]^T$, where H is the substrate height (GaAs, $\epsilon_r=12.9$). Here, $y = [L/H]$, which is given by

$$L/H = \mu_0 \ f(W/H, W_0/W, D/W) \quad (17)$$

hence, $\mathbf{x}_r = [W/H \ W_0/W \ D/W]^T$. A FIEM was developed in the range [2, 10] GHz. The region of interest is $1 < W/H < 2.2$, $0.2 < W_0/W < 1$ and $0.2 < D/W < 0.8$. We use a MRF_{3,2,2} to approximate L/H . The training points are chosen according to the Central Composite Design [9] in addition to 8 more points (total 23 training points). The parameters of the MRF are obtained by the Huber optimizer in OSA90/hope [13]. The percentage errors in the inductance L and in S_{11} at 30 test points are shown in Fig. 13. Fig. 14 compares the results obtained by the FIEM and those from Sonnet's *em* [11].

The results of the FIEM in the range [2, 22] GHz are shown in Fig. 15. We notice large errors at high frequencies. This is because the simple inductor to ground does not take into account the effect of the pad surrounding the via hole and the step junction [15] (see Fig. 12). To overcome this deficiency we develop a FDEM in the range [2, 22] GHz. The circuit model frequency (applying dimensional analysis and using the odd property of the frequency mapping) takes the same form as in (16). We use multivariable rational functions to approximate y as well as ω_c . The number of training points used is 23. The percentage errors in L and in S_{11} at 30 test points are shown in Figs. 16 (a) and (b), respectively. The

transformation of the FDEM into an equivalent FIEM follows the microstrip right angle bend example. The frequency ω_c is given by (8). The equivalent impedance of L is of the form of (9a). The resulting FIEM is shown in Fig. 17.

Microstrip Double-Step

Here, we consider broadband modeling of the microstrip double-step element in Fig. 18(a). It can be used to model microstrip tapered lines or nonuniform (in width) microstrip lines. The circuit model consists of two shunt capacitances and one series inductance (see Fig. 18(b)). The fine model is analyzed by Sonnet's *em* [11]. The vector of fine model parameters $\mathbf{x}_f = [W_1 \ W_2 \ W_3]^T$. The substrate height $H=25$ mil, the relative dielectric constant $\epsilon_r = 9.7$ and the length l (see Fig. 18(a)) is 5 mil. The circuit elements vector $\mathbf{y} = [L_1/H \ C_1/H \ C_2/H]^T$. The elements of \mathbf{y} are given by

$$L_1/H = \mu_0 \ f_1\left(\frac{W_2}{H}, \frac{W_2}{W_1}, \frac{W_3}{W_2}\right) \quad (18a)$$

$$C_1/H = \epsilon_0 \ f_2\left(\frac{W_2}{H}, \frac{W_2}{W_1}, \frac{W_3}{W_2}\right) \quad (18b)$$

$$C_2/H = \epsilon_0 \ f_3\left(\frac{W_2}{H}, \frac{W_2}{W_1}, \frac{W_3}{W_2}\right) \quad (18c)$$

hence, $\mathbf{x}_r = [W_2/H \ W_2/W_1 \ W_3/W_2]^T$. The circuit model frequency (applying dimensional analysis and using the odd property of the frequency mapping) takes the same form as in (16). A FDEM of the double-step element is developed in the frequency range [1, 41] GHz. The region of interest is $0.1 < W_2/H < 1$, $0.5 < W_2/W_1 < 0.9$ and $0.5 < W_3/W_2 < 0.9$. We use a $\text{MRF}_{3,2,2}$ to approximate each element of the vector \mathbf{y} and a $\text{MRF}_{4,2,2}$ to approximate ω_c with the order of $(\omega H/c)^2$ restricted to 1. The number of training points is 23. The parameters of the MRFs are obtained by the Huber optimizer in OSA90/hope [13]. The errors in S_{11} and S_{21} of the FDEM with respect to Sonnet's *em* [11] at 27 testing points in the region of interest are shown in Figs. 19 (a) and (b), respectively. To evaluate the FDEM of the double-step we consider an alternative model for the double-step element. This model is composed of a microstrip transmission line and 2 step junctions as shown in Fig. 20. The empirical models for the microstrip line and the 2 step junctions are taken from OSA90/hope. Figs. 21(a) and (b) show the errors

in S_{11} and S_{21} of this model with respect to Sonnet's *em* [11] at 27 testing points in the region of interest. It is clear from Figs. 19 and 21 that the FDEM outperforms the double-step model in Fig. 20.

The FDEM of the double-step element is used to model the linear tapered microstrip line in Fig. 22. The parameters of the tapered line are $L=150$ mil, $W_{in}=18$ mil, $W_{out}=2$ mil, $H=25$ mil and $\epsilon_r=9.7$. The input microstrip line has a characteristic impedance of 50 ohm and the output line has a characteristic impedance of 100 ohm. The linear tapered microstrip line can be modeled by cascading 30 double-step elements (each of length $l=5$ mil). The ABCD matrix of the tapered line is related to the ABCD matrices of the double-step elements by

$$\begin{bmatrix} A & B \\ C & D \end{bmatrix} = \prod_{i=1}^{30} \begin{bmatrix} A_i & B_i \\ C_i & D_i \end{bmatrix} \quad (19)$$

We analyzed the tapered line by three methods: by Sonnet's *em* [11] (the fine model), by cascading 30 double-step elements, where the FDEM is used to model each element and by cascading 30 elements where the alternative model of the double-step element in Fig. 20 is used. Fig. 23 compares the results obtained by the three methods.

CPW Step Junction

Here, we develop a FIEM for the CPW step junction in Fig. 24(a). The fine model is analyzed by Sonnet's *em* [11] and the circuit is the LC circuit [12] in Fig. 5(b). The vector of input parameters $\mathbf{x}_f = [W_1 \ W_2 \ G]^T$ and the vector of the circuit elements is $\mathbf{y} = [L_1/H \ L_2/H \ C/H]^T$, where

$$L_1 / H = \mu_0 \ f_1(W_1/H, W_2/W_1, G/W_1) \quad (20a)$$

$$L_2 / H = \mu_0 \ f_2(W_1/H, W_2/W_1, G/W_1) \quad (20b)$$

$$C / H = \epsilon_0 \ f_3(W_1/H, W_2/W_1, G/W_1) \quad (20c)$$

Therefore, \mathbf{y} is a function of $\mathbf{x}_r = [W_1/H \ W_2/W_1 \ G/W_1]^T$. The region of interest is $40 \mu\text{m} < W_1 < 120 \mu\text{m}$, $0.2 < W_2/W_1 < 0.8$ and $0.2 < G/W_1 < 1$ and the frequency range is [5, 50] GHz. The substrate height H is 635 μm and the relative dielectric constant is $\epsilon_r = 12.9$ (GaAs). The number of training points is 23. Each element of the vector \mathbf{y} is approximated by a rational function $\text{MRF}_{3,2,2}$. The parameters of the MRFs are

obtained by the Huber optimizer in OSA90/hope [13]. Figs. 25 (a) and (b) compares between the results obtained by *em* [11] and those by the CPW step junction FIEM at 27 test points in the region of interest. We notice that the CPW step junction FIEM gives good results in broad frequency range 5 GHz to 50 GHz. Therefore, we do not need to develop a FDEM for the CPW step junction. This means that the elements of the CPW step junction empirical model are frequency independent. Fig. 26 compares between the capacitance C extracted from the Z-parameters obtained by *em* [11] and that predicted by the FIEM at 6 test points in the region of interest.

VI. CONCLUSIONS

We present a unified computer-aided modeling methodology for developing broadband models of microwave passive components. Our approach integrates in a coherent way full-wave EM simulations, artificial neural networks, multivariable rational functions, dimensional analysis and frequency mapping. Two types of models are considered: frequency-independent and frequency-dependent empirical models. The latter can be transformed to the former if we use a rational function to approximate the frequency mapping. This is important since the frequency-independent empirical models are readily implementable in conventional circuit simulators. We also discussed the passivity condition of the frequency-dependent empirical models. We applied our modeling methodology to develop broadband models for several microwave components, including a microstrip right angle bend, a microstrip via, a microstrip double-step and a CPW step junction.

Appendix A

The passivity conditions for the FDEM can be proven as follows. The impedance in (9a) is written in terms of $s = j\omega$ as

$$Z_L(s) = L s \frac{f_1 + s^2 f_2}{f_3 + s^2 f_4} \quad (\text{A1})$$

By partial fraction we get

$$Z_L(s) = L \frac{f_2}{f_4} \left(1 + \frac{f_1/f_2 - f_3/f_4}{f_3/f_4 + s^2} \right) \quad (\text{A2})$$

Since the poles of an LC impedance lie on the $j\omega$ axis and have positive residues, we get the following

conditions

$$L \frac{f_2}{f_4} > 0 \quad (\text{A3})$$

$$f_3 / f_4 > 0 \quad (\text{A4})$$

$$f_1 / f_2 - f_3 / f_4 > 0 \quad (\text{A5})$$

The inductance L must be positive, hence, f_1, f_2, f_3, f_4 must have the same sign. If we assume that f_1, f_2, f_3, f_4 are positive, the conditions in (A3-A5) are equivalent to

$$f_i > 0, i = 1 \dots 4 \quad (\text{A6})$$

$$f_1 f_4 - f_2 f_3 > 0 \quad (\text{A7})$$

Those conditions can be also obtained by applying the same procedure on the impedance in (9b).

Appendix B

We apply dimensional analysis to determine the dependency of the circuit model frequency ω_c (in the microstrip right angle bend example) on the fine model frequency ω and the other parameters. The method of dimensional analysis is based on Buckingham's theorem [4]. This theorem states that "If an equation is dimensionally homogeneous it can be reduced to a relationship among a complete set of dimensionless products of the system variables". The dimensionless products are called Pi (π) terms [4,5]. For our case we assume that ω_c depends on ω , the device parameters W, H, ε , the free space permittivity ε_0 and the speed of light c (we can replace c with the free space permeability μ_0). A dimensional product π takes the form

$$\pi = H^{x_1} W^{x_2} c^{x_3} \varepsilon^{x_4} (\varepsilon_0)^{x_5} \omega^{x_6} (\omega_c)^{x_7} \quad (\text{B1})$$

where the x 's are evaluated by solving the system of homogeneous equations

$$\mathbf{C} \mathbf{x} = 0 \quad (\text{B2})$$

The elements of the coefficient matrix \mathbf{C} in (B2) can be obtained by constructing the table [4]

	x_1	x_2	x_3	x_4	x_5	x_6	x_7
	H	W	C	ε	ε_0	ω	ω_c
Kg	0	0	0	-1	-1	0	0
M	1	1	1	-3	-3	0	0
S	0	0	-1	4	4	-1	-1
A	0	0	0	2	2	0	0

where Kg, M, S and A are the units of the SI system. Therefore, \mathbf{C} is given by

$$\mathbf{C} = \begin{bmatrix} 0 & 0 & 0 & -1 & -1 & 0 & 0 \\ 1 & 1 & 1 & -3 & -3 & 0 & 0 \\ 0 & 0 & -1 & 4 & 4 & -1 & -1 \\ 0 & 0 & 0 & 2 & 2 & 0 & 0 \end{bmatrix} \quad (\text{B3})$$

The number of independent solutions of (B2) (the same as the number of independent π -terms) equals the number of elements of \mathbf{x} minus the rank of the matrix \mathbf{C} . In our case the number of elements of \mathbf{x} is 7 and the rank of the matrix \mathbf{C} is 3, hence we have 4 independent solutions of (B2) or 4 π -terms. These independent solutions are given in the table

x_1	x_2	x_3	x_4	x_5	x_6	x_7
1	0	-1	0	0	1	0
0	1	-1	0	0	1	0
0	0	0	-1	1	0	0
0	0	0	0	0	-1	1

Substituting the value of x 's in (B1) we get the following π -terms

$$\pi_1 = \omega H / c, \quad \pi_2 = \omega W / c, \quad \pi_3 = \varepsilon / \varepsilon_0 = \varepsilon_r, \quad \pi_4 = \omega_c / \omega \quad (\text{B4})$$

from π_1 and π_2 we can get $\pi_2' = \pi_2 / \pi_1 = W / H$. Applying Buckingham's theorem [4,5] the relation between the independent π -terms can take the form

$$\pi_4 = \varphi(\pi_1, \pi_2', \pi_3) \quad (\text{B5})$$

Therefore,

$$\omega_c = \omega \varphi(W/H, \varepsilon_r, \omega H/c) \quad (\text{B6})$$

But since ω_c is an odd function of ω (see Section III) we get

$$\omega_c = \omega f(W/H, \varepsilon_r, (\omega H/c)^2) \quad (\text{B7})$$

ACKNOWLEDGEMENT

The authors thank Dr. J.C. Rautio, President, Sonnet Software, Inc., Liverpool, NY, for making *em*TM available. The authors also appreciate the support of this work by the Natural Sciences and Engineering Research Council of Canada (NSERC) under Grants OGP0007239 and STP0201832, and through the Micronet Network of Centres of Excellence.

REFERENCES

1. A.H. Zaabab, Q.J. Zhang and M.S. Nakhala, A neural network modeling approach to circuit optimization and statistical design, IEEE Trans. Microwave Theory Tech., vol. 43, 1995, pp. 1349-1358.
2. P. Watson and K.C. Gupta, EM-ANN models for microstrip vias and interconnects in multilayer circuits, IEEE Trans. Microwave Theory Tech., vol. 44, 1996, pp. 2495-2503.
3. H. Leung and S. Haykin, Rational function neural network, Neural Computation, vol. 5, 1993, pp. 928-938.
4. W.H. Middendorf, Design of Devices and Systems. New York: Marcel Dekker, Inc., 1986, Chapter 7.
5. P. Watson, M.Y. Mah and L.L. Liou, Input variable space reduction using dimensional analysis for artificial neural network modeling, IEEE MTT-S Int. Microwave Symp. Dig. (Anaheim, CA), 1999, pp. 269-272.
6. J.W. Bandler, R.M. Biernacki, S.H. Chen, R.H. Hemmers and K. Madsen, Electromagnetic optimization exploiting aggressive space mapping, IEEE Trans. Microwave Theory Tech., vol. 43, 1995, pp. 2874-2882.
7. J.W. Bandler, M.A. Ismail, J.E. Rayas-Sánchez and Q.J. Zhang, Neuromodeling of microwave circuits exploiting space mapping technology, IEEE Trans. Microwave Theory Tech., vol. 47, 1999, pp. 928-938.
8. G.C. Temes and J.W. Lapatra, Introduction to Circuit Synthesis and Design. New York: McGraw-Hill, Inc., 1977.
9. D.C. Montgomery, Design and Analysis of Experiments. New York: Wiley, 1991.
10. R. Collin, Foundations for Microwave Engineering. New York: McGraw-Hill, Inc., 1966.
11. *em*TM Version 4.0b, Sonnet Software, Inc., 1020 Seventh North Street, Suite 210, Liverpool, NY 13088, 1997.
12. K.C. Gupta, R. Garg, I.J. Bahl, Microstrip Lines and Slotlines. Dedham, MA: Artech House, 1979.
13. OSA90/hopeTM Version 4.0, formerly Optimization Systems Associates Inc., P.O. Box 8083, Dundas, Ontario, Canada L9H 5E7, now Agilent Technologies, 1400 Fountaingrove, Parkway, Santa Rosa, CA 95403-1799.
14. M. Kirschning, R. Jansen and N. Koster, Measurement and computer-aided modeling of microstrip discontinuities by an improved resonator method, IEEE MTT-S Int. Microwave Symp. Dig. (Boston, MA), 1983, pp. 495-497.
15. D.G. Swanson, Jr., Grounding microstrip lines with via holes, IEEE Trans. Microwave Theory Tech., vol. 40, 1992, pp. 1719-1721.

TABLE I
EXPRESSIONS OF THE ELEMENTS OF THE FDEM
OF THE MICROSTRIP RIGHT ANGLE BEND

Element	Expression
$L/H(\text{nH/mil})$	$0.03192 \frac{-0.09 - 0.018x_1 + 0.3x_1^2}{1 + 2.853x_1^2}$
$C/H(\text{pF/mil})$	$0.000225(-0.46 + 0.162x_1 - 0.014x_2 + 0.275x_1^2 + 2.855x_1x_2 + 0.262x_1^2x_2)$
ω_c/ω	$\frac{f_1(x_1, x_2, x_3)}{f_2(x_1, x_2, x_3)}$
	$f_1(x_1, x_2, x_3) = 0.759 - 0.0192x_1 - 0.0179x_2 + 0.0187x_3 + 0.0738x_1^2 + 0.0026x_1x_2$ $- 0.1405x_1x_3 + 0.0079x_2x_3 + 0.0018x_1^3 - 0.0071x_1^2x_2 + 0.1188x_1^2x_3$ $+ 0.0017x_1x_2^2 + 0.0419x_1x_2x_3 - 0.0022x_2^2x_3$
	$f_2(x_1, x_2, x_3) = 1 + 0.0282x_1 - 0.0086x_2 - 0.0175x_3 + 0.0051x_1^2 - 0.0063x_1x_2$ $+ 0.1674x_1x_3 + 0.0037x_2^2 - 0.0067x_2x_3 + 0.0055x_1^3 - 0.0028x_1^2x_2$ $+ 0.0011x_1^2x_3 + 0.0056x_1x_2x_3 - 0.0012x_2^2x_3$
	where $x_1 = W/H$, $x_2 = \epsilon_r$, $x_3 = 1.816e-7 (\omega(\text{GHz})H(\text{mil}))^2$

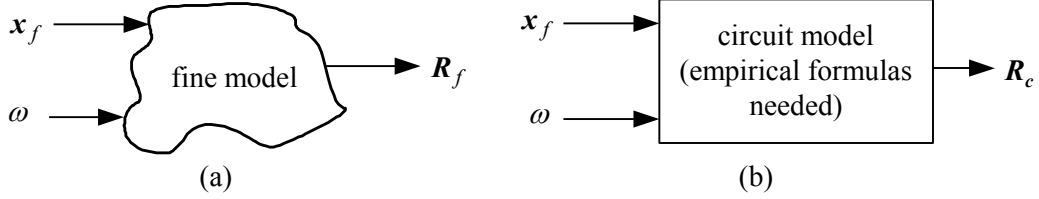


Fig. 1. The fine model (a) and the circuit model (b).

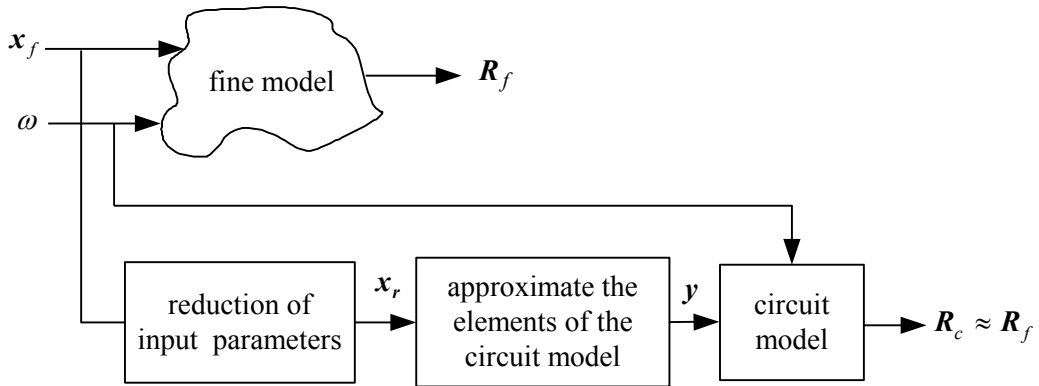


Fig. 2. The development of the frequency-independent empirical models.

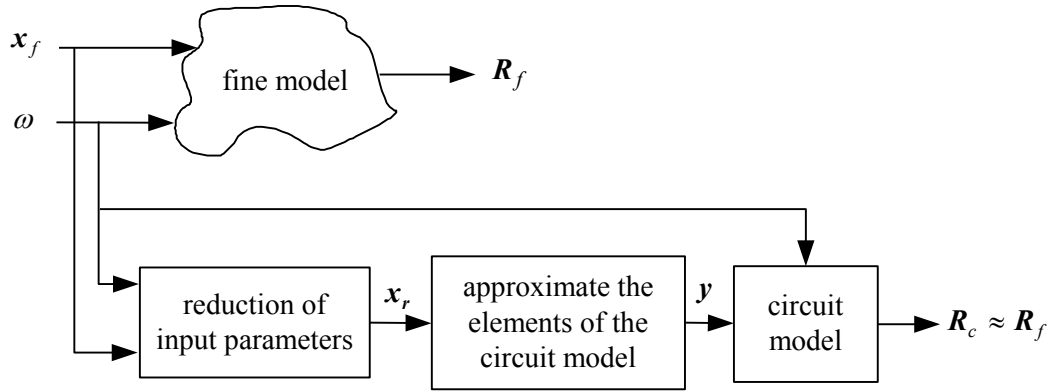


Fig. 3. The development of the frequency-dependent empirical models with circuit model elements explicitly function of frequency.

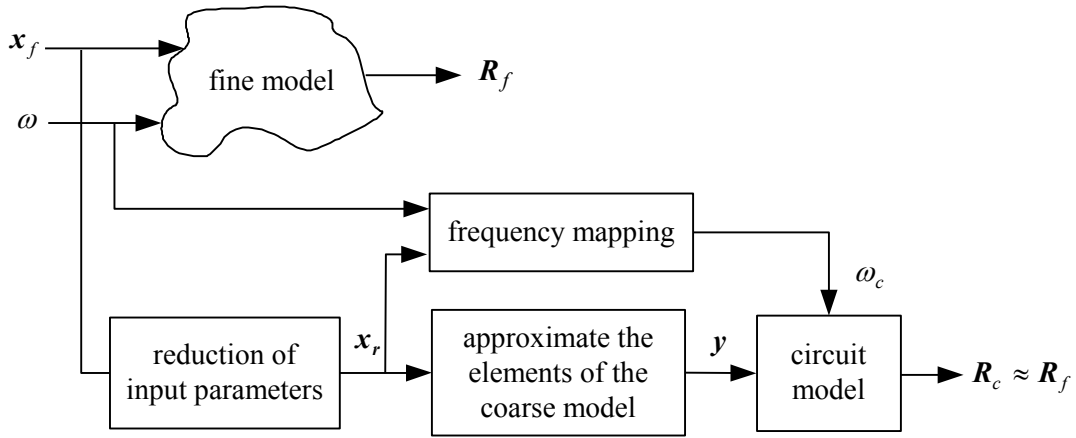


Fig. 4. The development of the frequency-dependent empirical models with the circuit model elements implicitly function of frequency through frequency mapping.

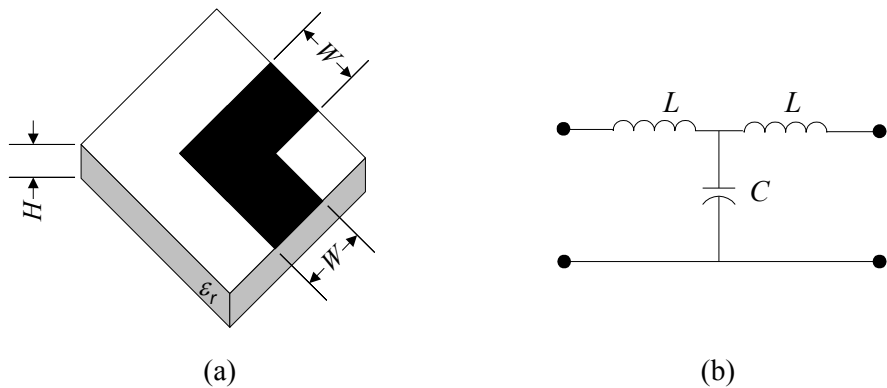


Fig. 5. The microstrip right angle bend: (a) the fine model, (b) the circuit model.

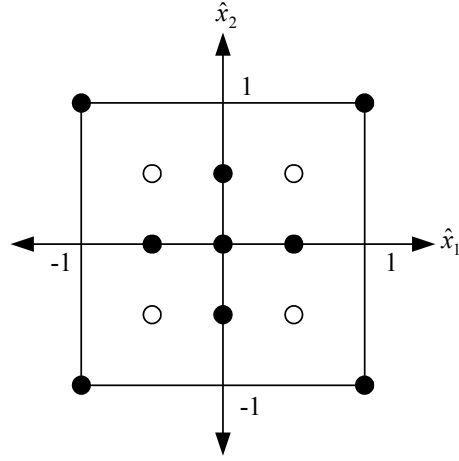


Fig. 6. The training points for the microstrip right angle bend.

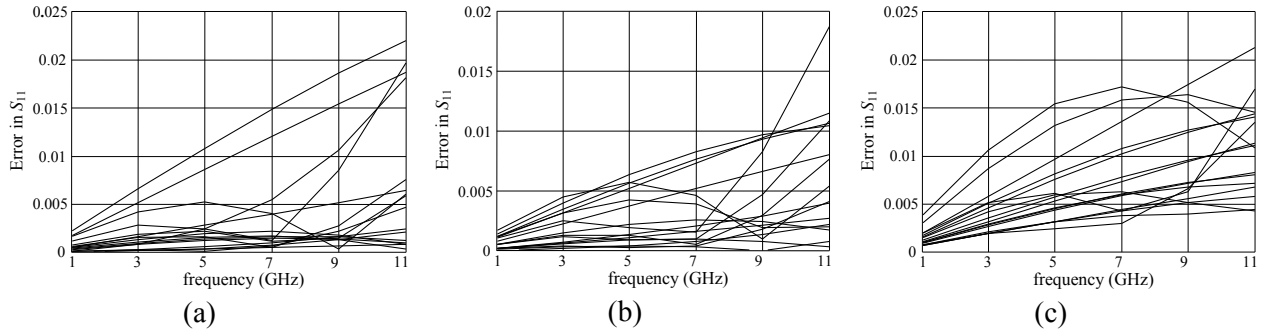


Fig. 7. The error in S_{11} of the microstrip right angle bend with respect to em^{TM} at the test points: (a) the FIEM developed by ANNs, (b) the FIEM developed by MRFs, (c) by the empirical model in [14].

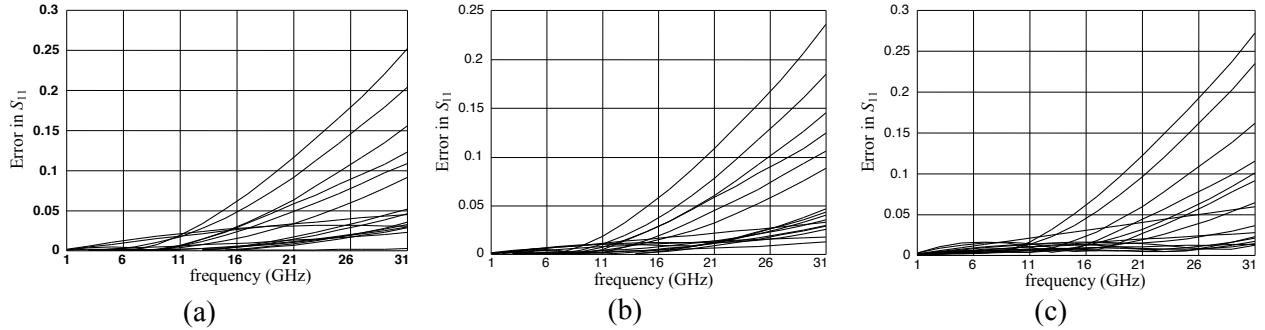


Fig. 8. The error in S_{11} of the microstrip right angle bend with respect to em^{TM} over a broad frequency range: (a) the FIEM developed by ANNs, (b) the FIEM developed by MRFs, (c) the empirical model in [14].

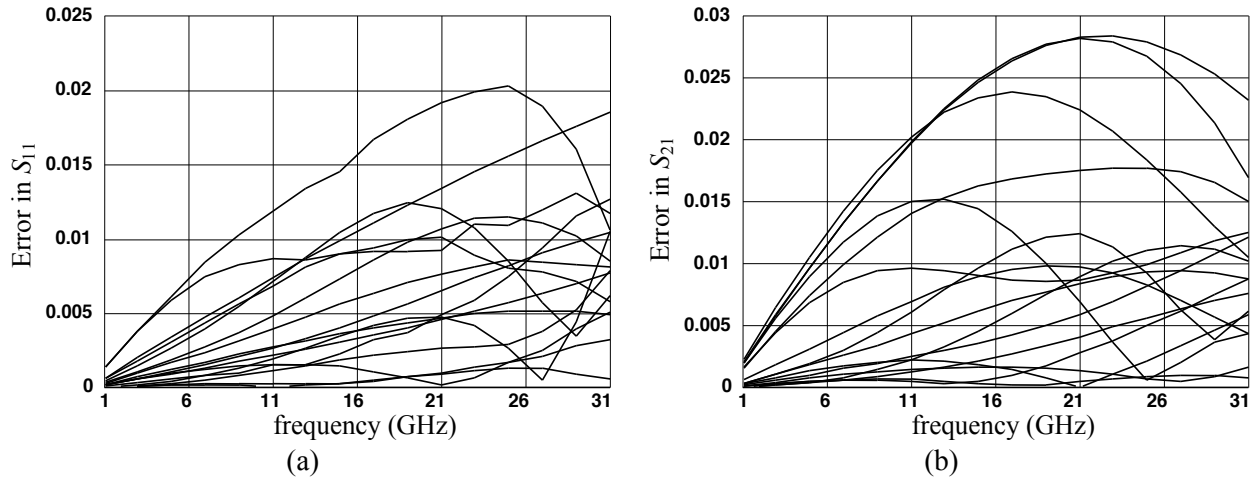


Fig. 9. The error of the FDEM of the microstrip right angle bend (developed by MRFs) with respect to em^{TM} at the test points: (a) in S_{11} , (b) in S_{21} .

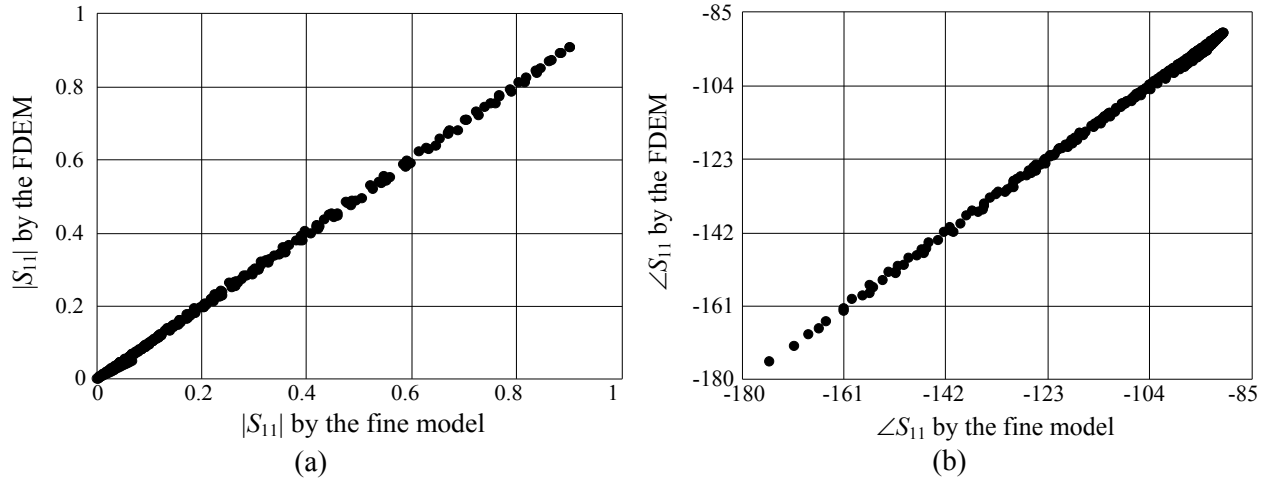
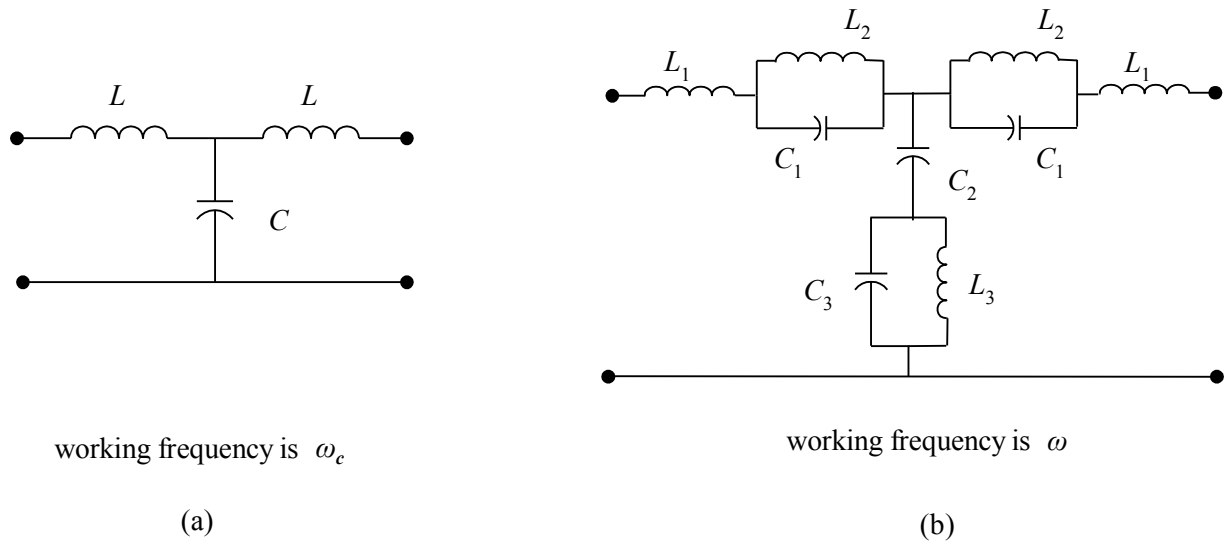
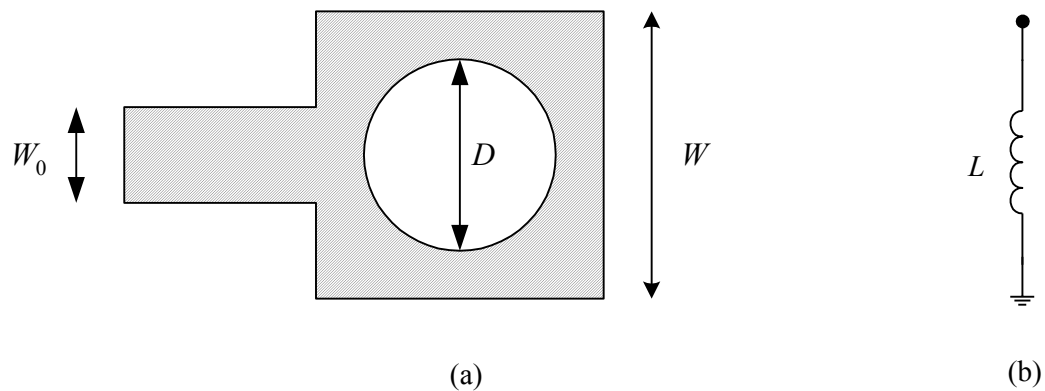


Fig. 10. Comparison between the responses obtained by the FDEM of the microstrip right angle bend and those obtained by em^{TM} at the test points: (a) magnitude of S_{11} , (b) phase of S_{11} in degrees.



(a) (b)
 Fig. 11. The FDEM of the microstrip right angle bend (a) and the equivalent FIEM (b).



(a) (b)
 Fig. 12. The microstrip via: (a) the physical structure, (b) the circuit model.

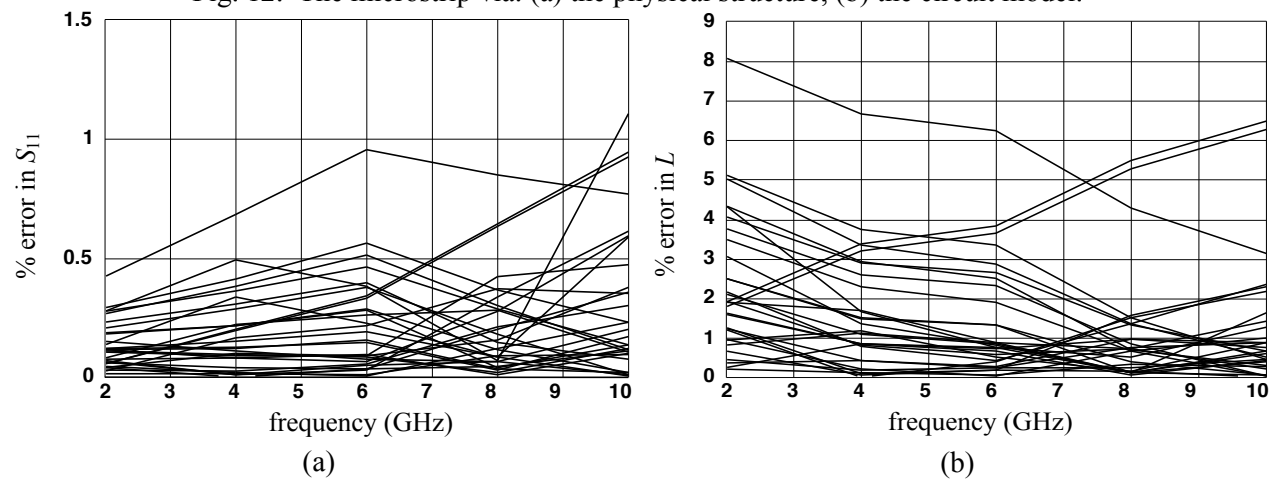


Fig. 13. Percentage error of the FIEM of the microstrip via with respect to *em*TM at the test points: (a) in *S*₁₁, (b) in *L*.

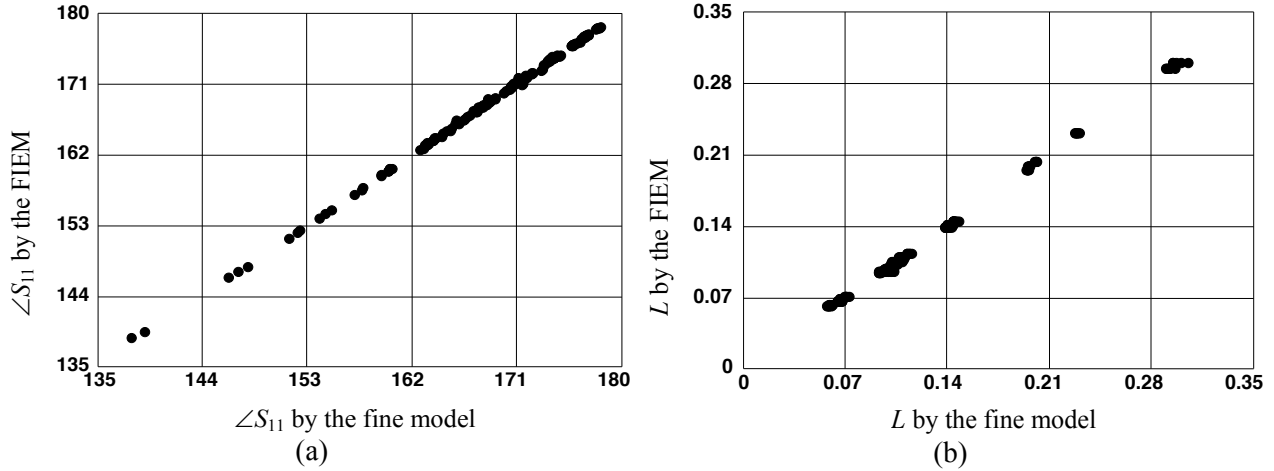


Fig. 14. Comparison between the responses obtained by the FIEM of the microstrip via and those obtained by em^{TM} at the test points in the frequency range [2, 10] GHz: (a) phase of S_{11} , (b) the inductance L .

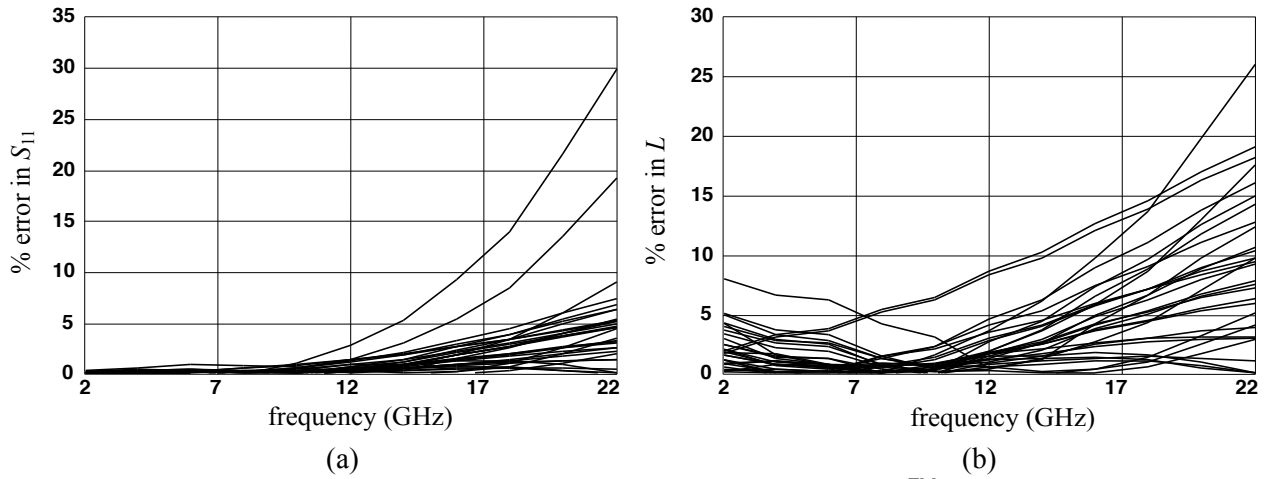


Fig. 15. Comparison of the FIEM of the microstrip via with respect to em^{TM} over a broad frequency range at the test points: (a) % error in S_{11} , (b) % error in L .

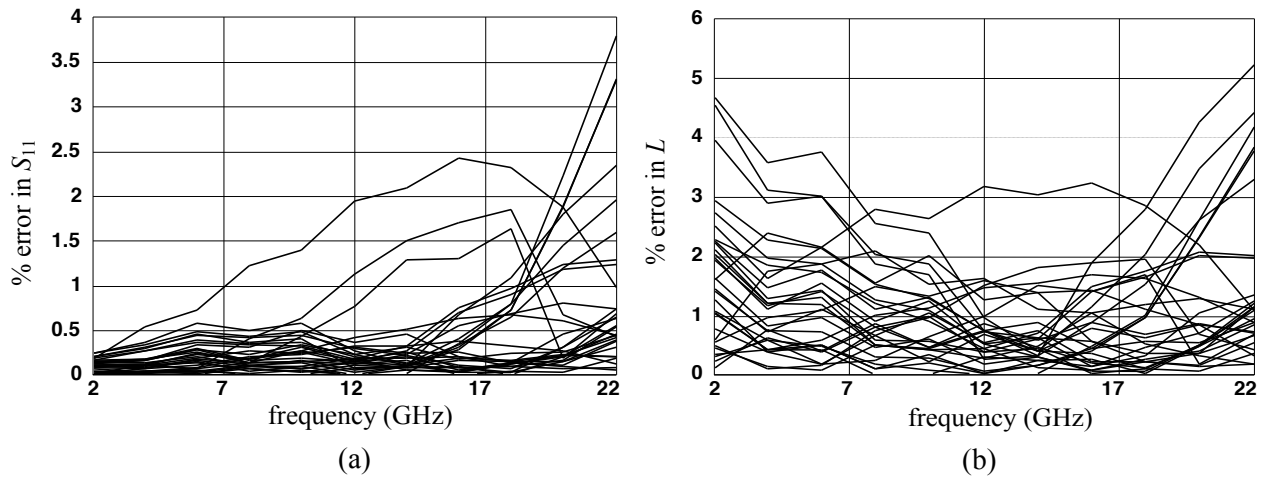


Fig. 16. Comparison of the FDEM of the microstrip via with respect to em^{TM} over a broad frequency range at the test points: (a) % error in S_{11} , (b) % error in L .

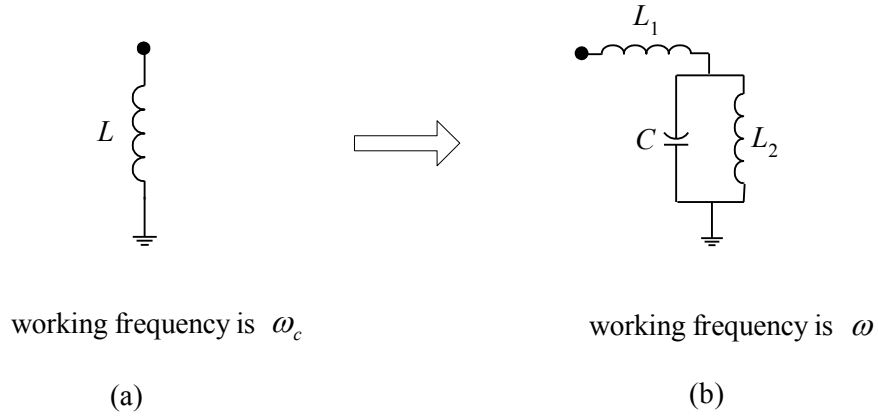


Fig. 17. The FDEM of the microstrip via (a) and the corresponding FIEM (b).

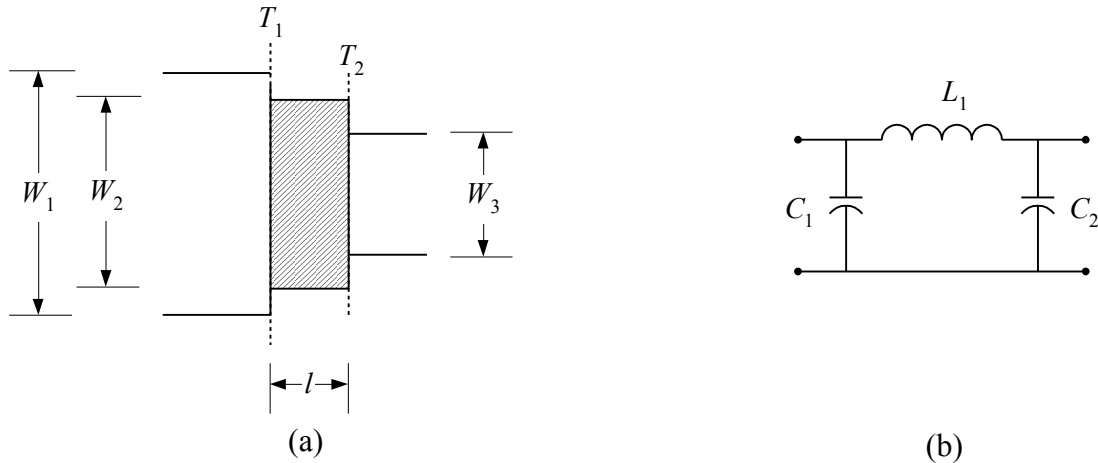


Fig. 18. The microstrip double-step: (a) the physical structure where T_1 and T_2 are the reference planes, (b) the circuit model.

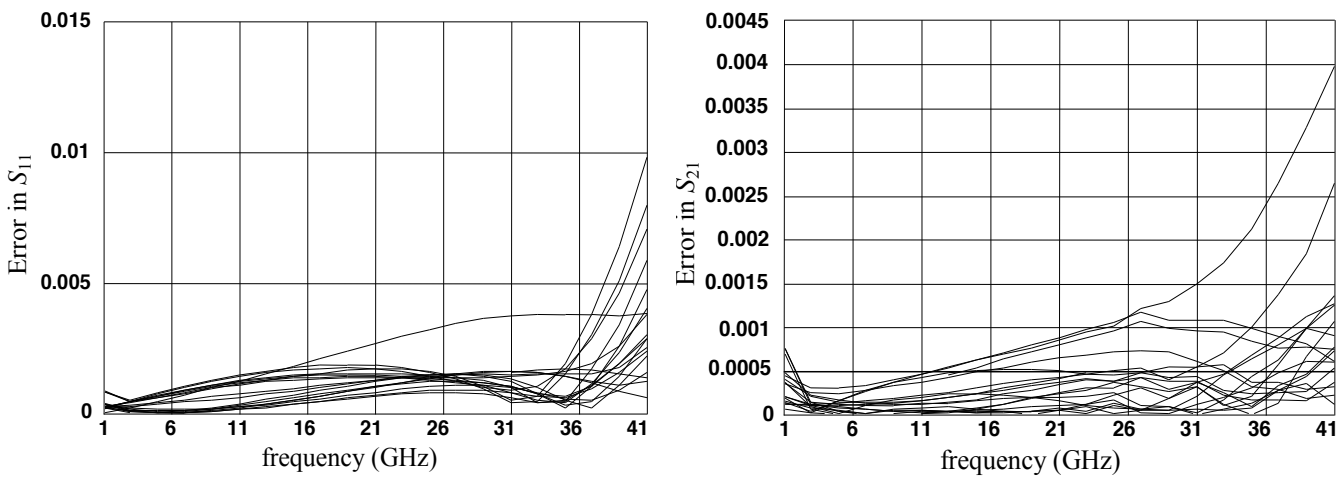


Fig. 19. Comparison between the FDEM of the double-step element and em^{TM} at the test points in the region of interest: (a) error in S_{11} , (b) error in S_{21} .

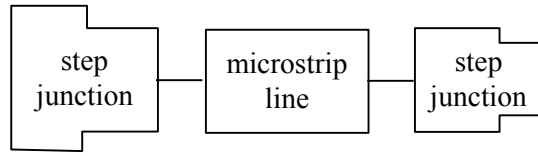


Fig. 20. An alternative model for the microstrip double-step element.

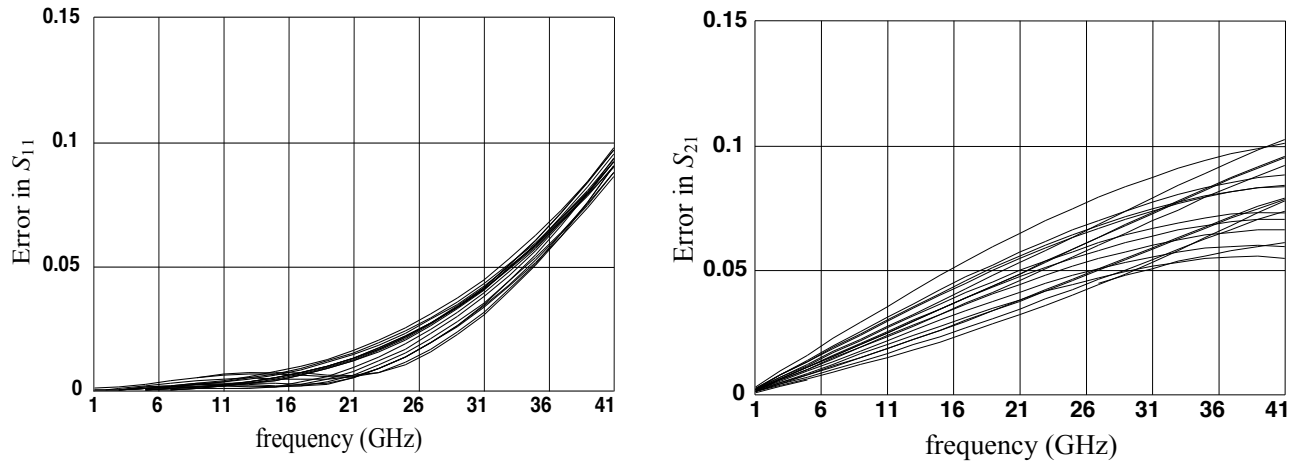


Fig. 21. Comparison between the double-step model in Fig.20 and em^{TM} at the test points in the region of interest: (a) error in S_{11} , (b) error in S_{21} .

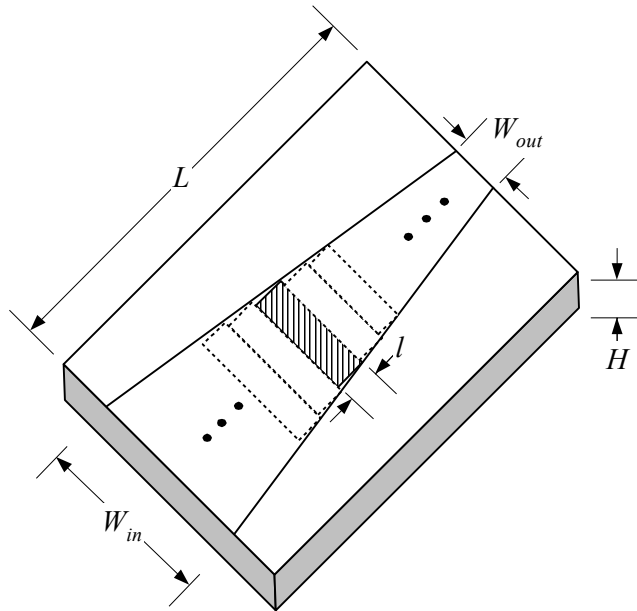


Fig. 22. Linear tapered microstrip line.

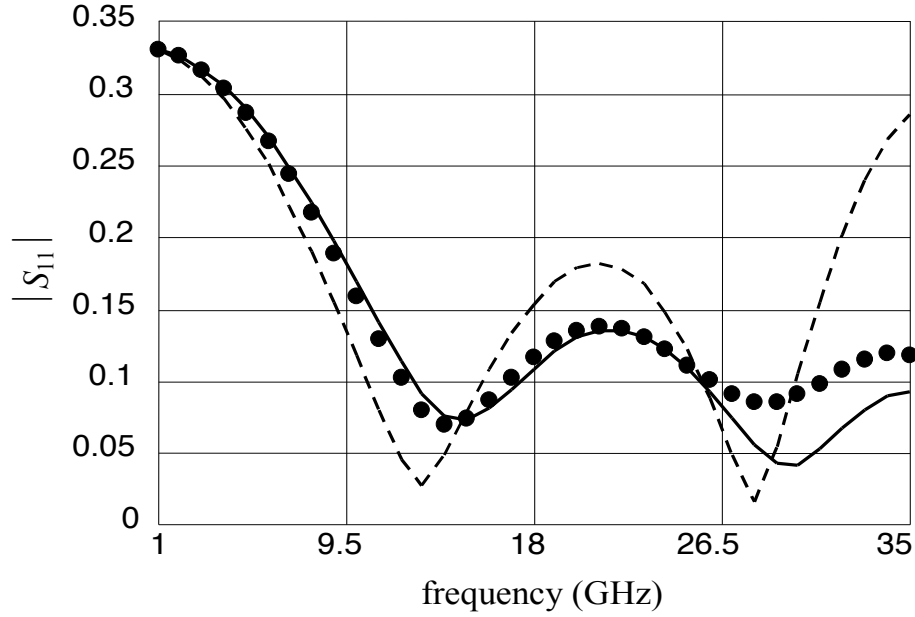


Fig. 23. The response of the linear tapered microstrip line by em^{TM} ($\bullet \bullet$), by the FDEM of the double-step element (—), by the model in Fig.20 of the double-step element (----).

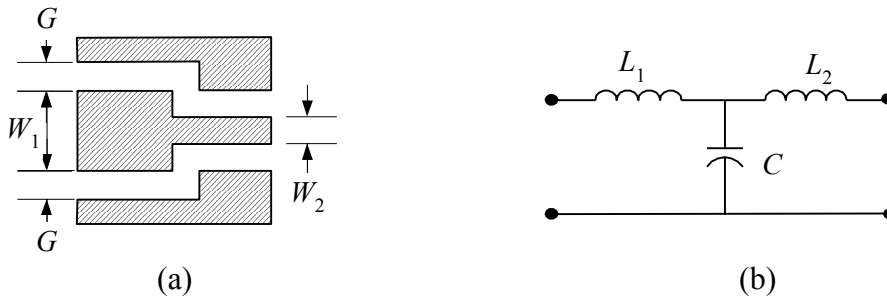


Fig. 24. The CPW step junction: (a) the physical structure, (b) the circuit model.

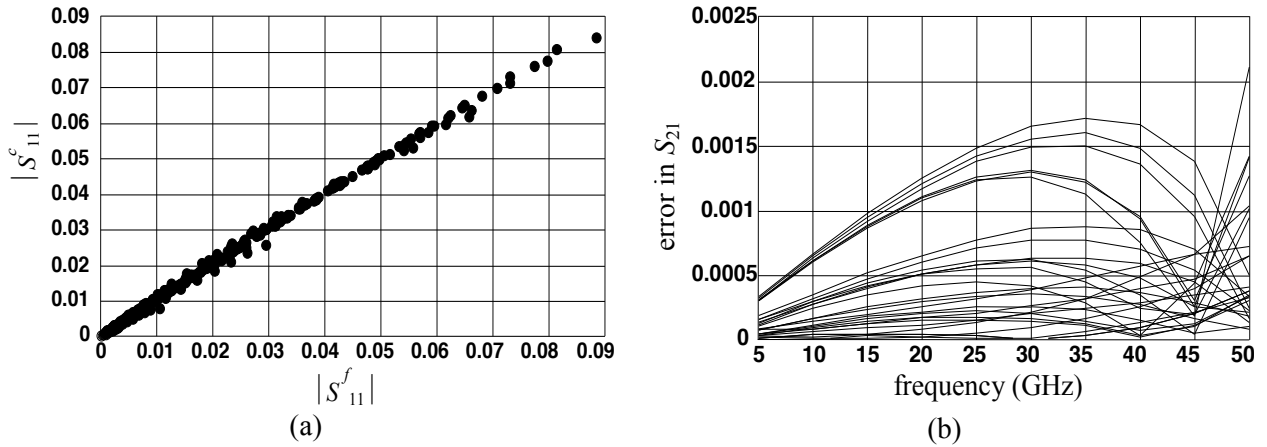


Fig. 25. Comparison between the results obtained by em^{TM} and by the FIEM of the CPW step junction: (a) $|S_{11}|$ by em^{TM} versus that of the FIEM, (b) the error in S_{21} .

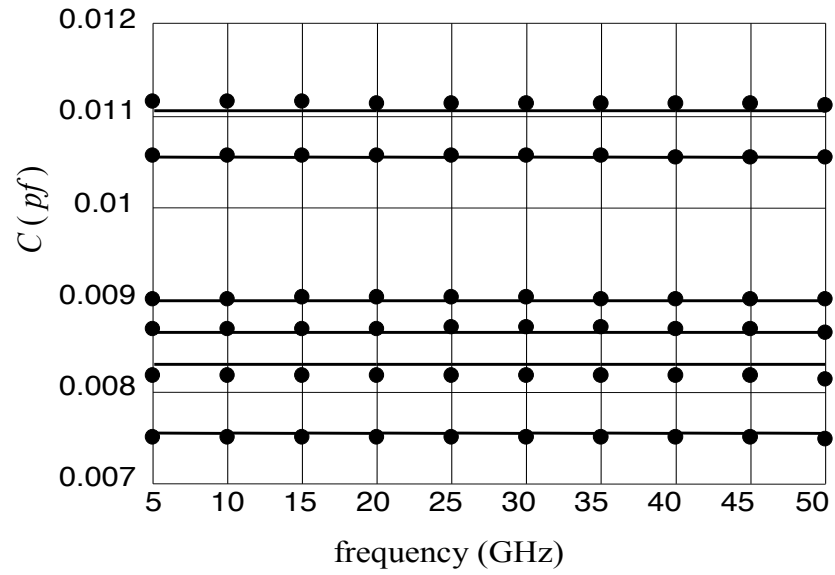


Fig. 26. The capacitance of the CPW step junction: (a) extracted from the fine model (••), (b) predicted by the FIEM of the CPW step junction (—).